Fachtagung "Lasermethoden in der Strömungsmesstechnik"
8. – 10. September 2015, Dresden

Rohrströhmungsverhalten bei Drallerzeugung: Validierung von CFD Simulationen mit Laser-Doppler Anemometrie

Characteristics of pipe-flow subject to swirl disturbances: Validation of CFD simulations with laser-Doppler velocimetry

Simon Graner[12], Diego del Olmo Díaz[1], Denis F. Hinz[1], and Christian Breitsamter[2]
[1]Kamstrup A/S, Industrivej 28, Stilling 8660 Skanderborg, Denmark
[2]Lehrstuhl für Aerodynamik und Strömungsmechanik, Technische Universität München, Boltzmannstrasse 15, 85748 Garching b. München, Germany

Laser-Doppler Anemometrie, Drallerzeuger, Numerische Strömungssimulation, Validierung
Laser-Doppler velocimetry, swirl disturbance generator, computational fluid dynamics, validation

Summary

We study characteristic flow patterns downstream of a standardized swirl disturbance generator using laser-Doppler velocimetry (LDV) and computational fluid dynamics (CFD). To investigate the spatial development of flow patterns, we conduct LDV measurements in cross-sections located at various distances downstream from the swirl disturbance generator. Focusing on velocity profiles and performance indicators, we systematically compare experimental results with the corresponding CFD simulations. Hereby, we validate various turbulence models and assess the potential to predict the experimental data with numerical simulations. The realizable k-ε model shows good agreement with the experimental results and an acceptable prediction of the performance indicator K_p and the swirl angle ϕ compared to experiments, literature references (Eichler and Lederer 2015, Müller and Dues 2007), and theory (Gersten and Papenfuss 2005).

Introduction

LDV has significant potential to study pipe-flows and thereby assist the design and validation of commercial flow meters. New meters are usually tested for a wide range of operating conditions including various flow rates, temperatures, and artificially generated flow disturbances. In particular swirling flow may compromise the accuracy of the meter reading. Therefore, it is of key relevance to explore the underlying flow-physics. With the objective of achieving better understanding of swirling flows, we perform LDV experiments and CFD simulations with a standardized swirl disturbance generator (EN 14154-3:2005 and OIML R 49-2:2013). To investigate the spatial development of the swirling wake, we collect LDV data at various measurement sections downstream from the swirl disturbance generator. CFD simulations are realized with a Reynolds-averaged Navier–Stokes (RANS) approach and systematically compared to experiments with the goal of assessing the performance of different turbulence models to predict disturbed flow patterns in pipe-flow applications.

Materials and methods

Test bench and LDV system

We perform all experiments on a verification and calibration test bench in the flow laboratory of Kamstrup A/S using brass pipes of inner diameter $D = 15.0\,\mathrm{mm}$ and a water temperature of $T = 20\,°\mathrm{C}$. The standardized swirl disturbance generator is installed at least $100.0D$ downstream from the inlet of the test section to ensure undisturbed fully-developed upstream flow conditions. The volumetric flow rate Q, the water temperature T, and the pressure p are actively controlled and adjusted within a PID feedback loop. We consider Reynolds numbers $Re = 6.0 \cdot 10^4$, $Re = 4.0 \cdot 10^4$, and $Re = 1.0 \cdot 10^3$, which correspond to volumetric flow rates of $Q = 2.556\,\mathrm{m^3/h}$, $Q = 1.76\,\mathrm{m^3/h}$, and $Q = 0.0426\,\mathrm{m^3/h}$, where

$$Re = w_{vol} D/\nu \tag{1}$$

is the Reynolds number based on the volumetric velocity $w_{vol} = 4Q/\pi D^2$ and the kinematic viscosity $\nu = 1.004 \cdot 10^{-6}\,\mathrm{m^2/s}$. Further, we conduct LDV measurements in cross-sections $12.0D$, $50.0D$, and $105.0D$ downstream of the swirl disturbance generator. Flow perturbations are generated with a standardized clockwise swirl disturbance generator, as shown in Figure 1 (a). We use a commercial LDV probe from ILA/Optolution with a window chamber that enables full three-dimensional optical access for the measurement of all three velocity components. The probe is mounted on a traversing system for automated displacement in a Cartesian coordinate system. The traversing system is installed on the side of the window chamber to measure the axial velocity component as well as the velocity component in y-direction and on top to measure the velocity component in x-direction. Figure 1 shows the clockwise swirl disturbance generator in panel (a), the LDV probe in panel (b), and the associated measurement grid in panel (c).

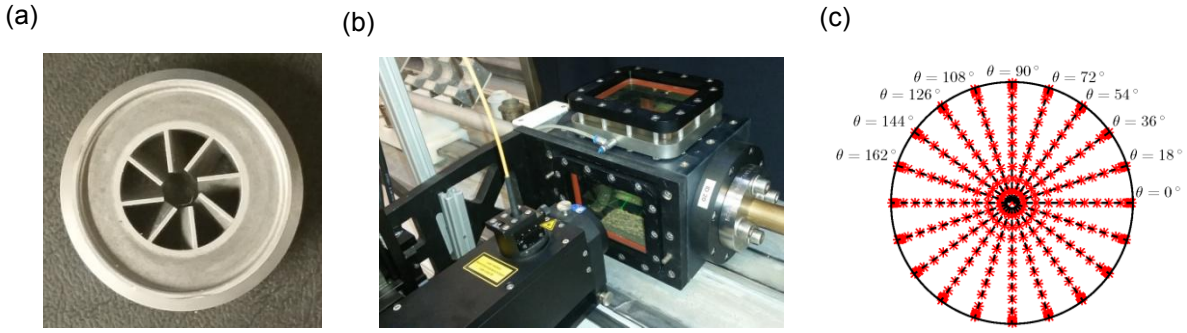

Figure 1: Clockwise swirl disturbance generator according to EN 14154-3:2005 and OIML R 49-2:2013 (a), the LDV probe (b), and the associated LDV measurement grid (c).

CFD simulations

The numerical simulations are performed with the open-source CFD code OpenFOAM. We use a RANS modeling approach and a hex-dominant unstructured mesh generated with the OpenFOAM utility *snappyHexMesh*. Different mesh sizes are tested and full results are reported in detail elsewhere (del Olmo Díaz and Hinz 2015). Throughout this article, we discuss simulation results for $Re = 4.0 \cdot 10^4$ combined with a mesh of approximately $20 \cdot 10^6$ cells. To identify best-practice guidelines for practical turbulence modeling, we test five dif-

ferent turbulence models: k-ε, realizable k-ε, RNG k-ε, k-ω and k-ω SST. The computational domain covers a distance of $13.0D$ downstream from the swirl disturbance generator.

Results

Velocity profiles

Contour plots of the axial velocity component and the magnitude $v_{xy} = \sqrt{\bar{u}^2 + \bar{v}^2}$ of the velocity component in the xy-plane for $Re = 4.0 \cdot 10^4$ are shown in Figure 2. The experimental results are measured at cross-sections $12.0D$ (Figure 2 (a) and (d)), $50.0D$ (Figure 2 (b) and (e)), and $105.0D$ (Figure 2 (c) and (f)) downstream from the swirl disturbance generator. In the measurement section at $12.0D$, we find an axial velocity profile with a nearly flat core region combined with high velocity gradients near the wall (Figure 2 (a)). Further downstream, the axial velocity profile evolves from a flat profile to a less disturbed moderately flat profile at $50.0D$ (Figure 2 (b)), and finally to a nearly fully-developed profile at the $105.0D$ measurement section (Figure 2 (c)).

The velocity contours of the secondary flow show an overall decrease with increasing distance between the swirl generator and the LDV measurement section. Our results indicate that v_{xy} vanishes at around $105.0D$ downstream from the swirl disturbance generator (Figure 2 (f)). The maximal magnitudes of the secondary flow are found in the measurement section at $12.0D$ at the outer part of the core-region (Figure 2 (e)). We also provide contour plots from simulations with the realizable k-ε model (Figure 3 (b) and (d)). The measured axial and radial velocity profiles appear more asymmetrical than predicted by the simulations with the realizable k-ε model (Figure 3 (b) and (d)). The asymmetries in the measurements include contributions associated with uncertainties in the positioning of the axial pipe center. Additionally, asymmetries as a result of flow instabilities are not captured in the steady-state RANS simulations. The experimental results show higher local peaks in the secondary flow close to the wall. This underestimation of the secondary flow appears consistently over the entire profile, but the overall flow structures are accurately captured by the realizable k-ε model. Aside from experiments with $Re = 4.0 \cdot 10^4$, we analyze the experiments with $Re = 6.0 \cdot 10^4$ (turbulent) and $Re = 1.0 \cdot 10^3$ (laminar) to inspect the self-similarity of flow structures across different flow rates. The turbulent pipe-flow with $Re = 6.0 \cdot 10^4$ shows axial and radial velocity profiles similar to the ones of the $Re = 4.0 \cdot 10^4$ case. Additionally, we find qualitatively similar asymmetries for $Re = 4.0 \cdot 10^4$ and $Re = 6.0 \cdot 10^4$ at the $12.0D$ and the $50.0D$ measurement sections. In contrast, the axial velocity profile in the laminar case is less flat and a smaller region in the pipe center appears to attain the peak velocity. The secondary flow reaches lower values than for $Re = 4.0 \cdot 10^4$ and $Re = 6.0 \cdot 10^4$. This confirms that swirl disturbances decay rapidly for laminar flow conditions.

In panel (a) of Figure 4, we show a comparison of individual axial velocity profiles at different downstream distances ($12.0D$, $50.0D$, and $105.0D$) along with the simulation of the realizable k-ε model at $12.0D$ and the Gersten & Herwig reference profile (Gersten and Herwig 1992) for a fully-developed turbulent pipe-flow. Analogous data for the y-component of the secondary flow is shown in panel (b) of Figure 4. In panel (a) of Figure 4, the peak velocity at $105.0D$ takes values around $\bar{w}/w_{vol} \approx 1.2$, signalizing compliance with an almost fully-developed flow profile. The secondary flow profiles show peaks at the outer core region and a linear radial dependency within the core region. This indicates that the swirling flow in the core region has a characteristic motion pattern close to a solid body rotation.

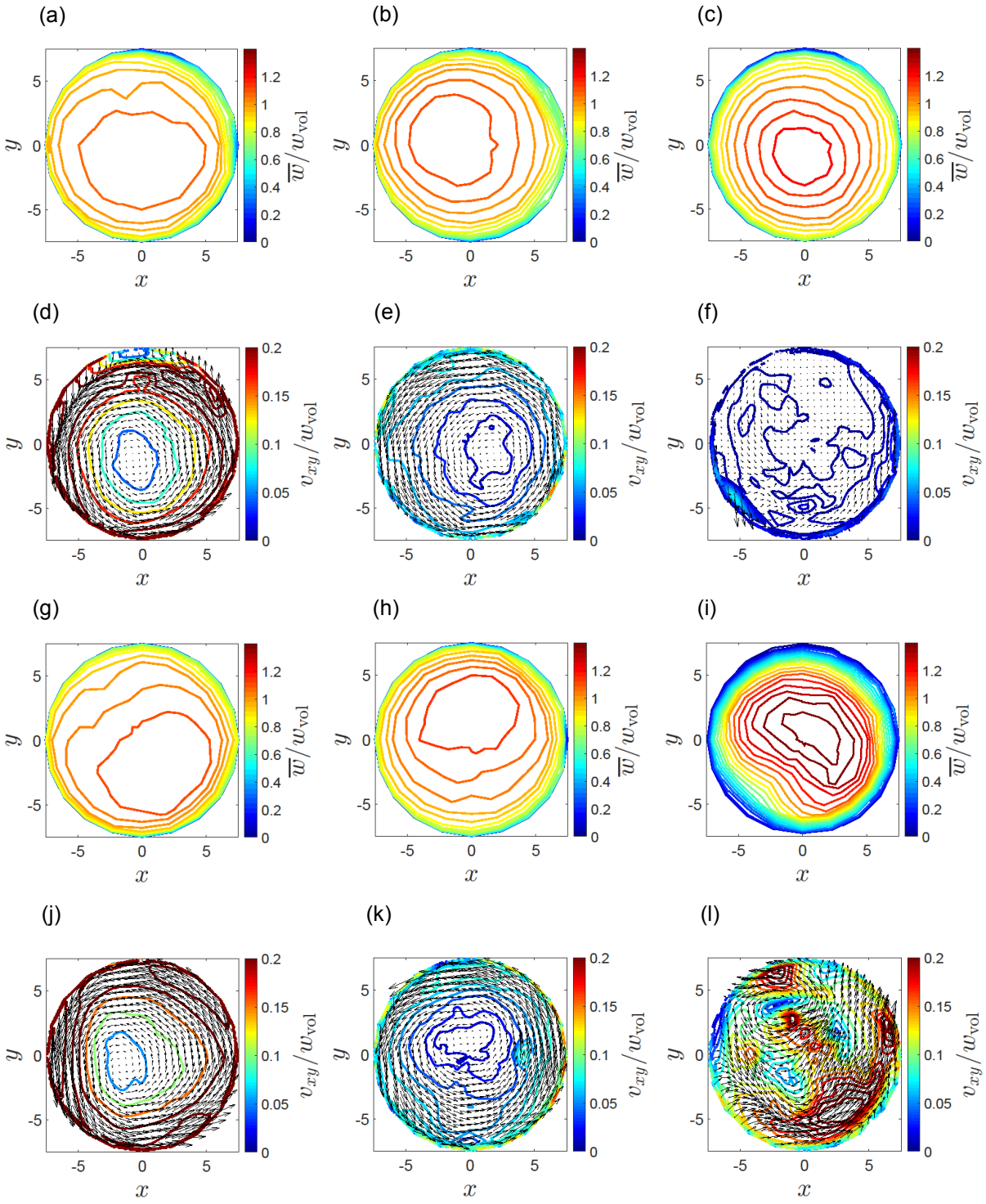

Figure 2: Comparison of axial and radial velocity profiles at different distances downstream from the swirl disturbance generator and different Reynolds numbers: $12.0D$ and $Re = 4.0 \cdot 10^4$: (a) and (d); $50.0D$ and $Re = 4.0 \cdot 10^4$: (b) and (e); $105.0D$ and $Re = 4.0 \cdot 10^4$: (c) and (f); $12.0D$ and $Re = 6.0 \cdot 10^4$: (g) and (j); $50.0D$ and $Re = 6.0 \cdot 10^4$ (h) and (k); $12.0D$ and $Re = 1.0 \cdot 10^3$: (i) and (l).

The realizable k-ε model provides reasonable approximations of the experimental axial and secondary flow profiles. However, it underpredicts the peaks in the secondary flow. The comparison in Figure 4 (a) shows that the axial velocity profile converges to the Gersten & Herwig reference profile with increasing distance from the swirl disturbance generator. The asymmetry persists for the measurements at the $50.0D$ and $105.0D$ downstream sections.

The secondary flow decreases rapidly and nearly vanishes at $105.0D$, which implies that a fully-developed profile is guaranteed after a distance of $105.0D$ downstream from the swirl disturbance generator.

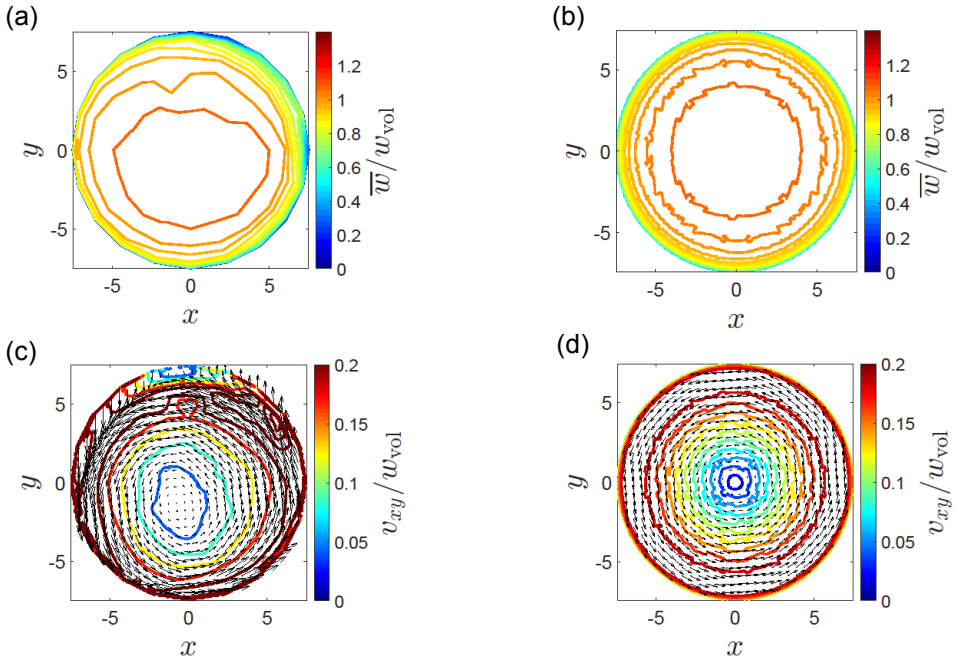

Figure 3: Comparison of axial and radial velocity profiles at $12.0D$: Experimental results ((a) and (c)) and simulation results ((b) and (d)) using the realizable k-ε model.

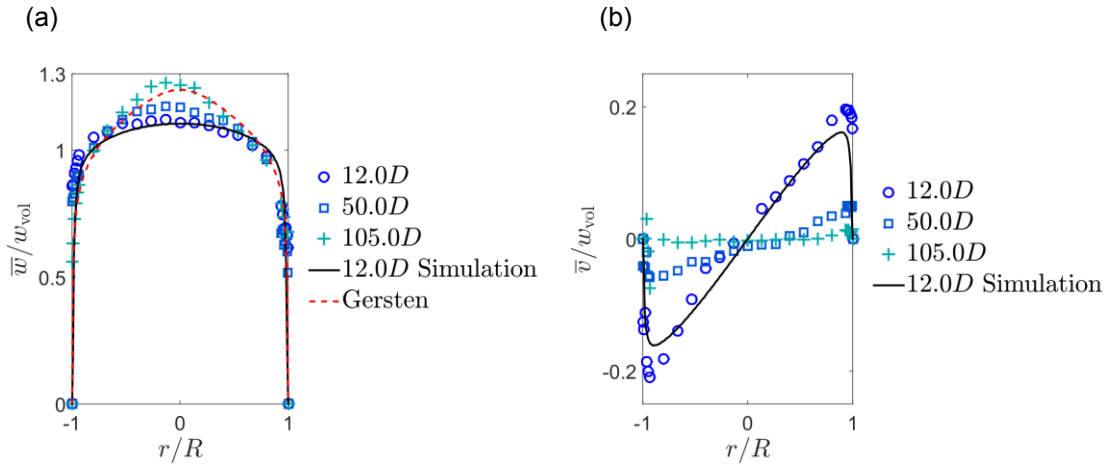

Figure 4: Comparison of the axial velocity profile (a) and the y-component of the secondary flow (b) at various distances downstream from the swirl disturbance generator with CFD simulations at $12.0D$ and the reference profile for fully-developed turbulent flow according to Gersten and Herwig 1992.

Performance indicators

To systematically compare the experimental, computational, and theoretical flow profiles, we use performance indicators (see, for example, Eichler and Lederer 2015). Performance indicators are useful integral metrics to quantify flow conditions. Following Yeh and Mattingly 1994 and Müller and Dues 2007, we compute the swirl angle ϕ, the profile factor K_p, the asymmetry factor K_a, and the turbulence factor K_{Tu}. To assess the performance indicators, we include the established limits for a sufficiently fully-developed flow profile according to

Eichler and Lederer 2015. We also compute the standard deviation of performance indicators determined from individual profiles on the measurement grid (Figure 1 (b)) and report them through error bars in Figure 5.

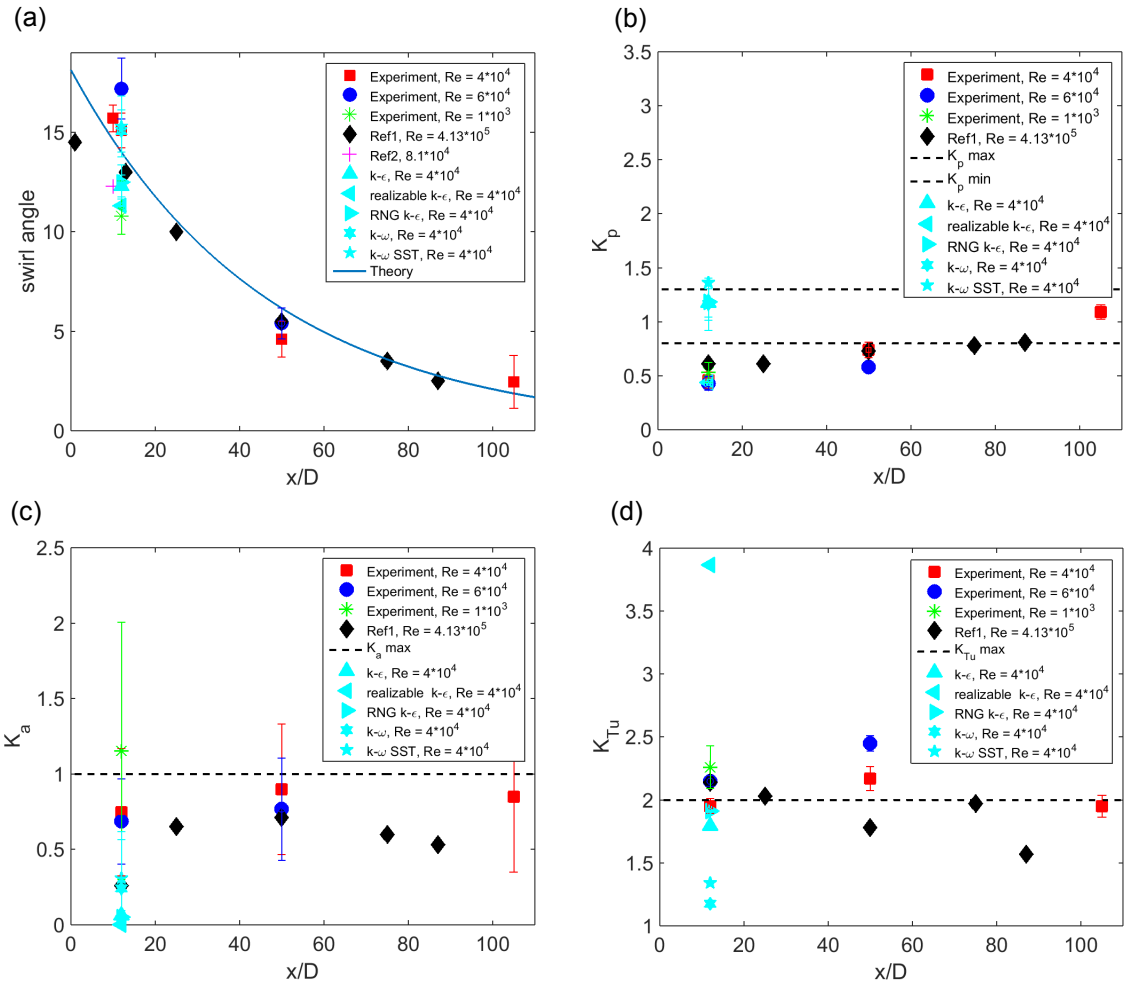

Figure 5: Comparison of flow profile performance indicators from LDV experiments, CFD simulations, and references: Swirl angle ϕ (a), profile factor K_p (b), asymmetry factor K_a (c), and turbulence factor K_{Tu} (d).

Figure 5 (a) shows a comparison of the swirl angle for experiments with three different Reynolds numbers, two references from the literature (Ref1: Eichler and Lederer 2015, Ref2: Müller and Dues 2007), the theory (Gersten and Papenfuss 2005) and simulations with various turbulence models. The theory after Gersten and Papenfuss 2005 suggests an exponential decay of disturbances in turbulent pipe-flow based on solving the incompressible Navier–Stokes equations with an asymptotic expansion approach. Adopting the theory of Gersten and Papenfuss 2005 for a single longitudinal vortex, we assume that the swirl angle ϕ is a suitable measure for the swirling intensity, such that the downstream decay is approximated by

$$\phi \sim \phi_o \cdot \mathrm{e}^{-\alpha\left(\frac{x}{D}-12.0\right)}, \tag{2}$$

where $\phi_o = 14°$ is the magnitude of the swirl angle associated with the boundary condition at $x/D = 12.0$, and α is the non-dimensional rate of decay. In the special case of a single longitudinal vortex, the rate of decay is proportional to the dimensionless friction factor λ such

that $\alpha = \lambda$. The empirical relationship $1/\sqrt{\lambda} = 1.869 \log\left(Re\sqrt{\lambda}\right) - 0.241$ for high Reynolds numbers (Zagarola and Smits 1998) yields $\lambda = 0.0216$ for $Re = 4.0 \cdot 10^4$. The experimental results at $Re = 4.0 \cdot 10^4$ and the Results from Eichler and Lederer 2015 show a good agreement with the single longitudinal vortex theory. Further, the measurements with $Re = 6.0 \cdot 10^4$ suggest that a higher Reynolds number leads to an increased swirl angle in the measurements section close to the swirl disturbance generator, but converges to similar swirl angles further downstream. The swirl angle at $10.0D$ measured by Müller and Dues 2007 appears to be lower than the other experimental values. When comparing the simulation results of various turbulence models, we find a spread of approximately $4°$ between different solutions, which is satisfactory, considering the experimental measurement uncertainty illustrated through the error bars. The two k-ω models and the k-ε model perform best whereas the realizable k-ε model provides a less accurate approximation of the swirl angle in comparison to theory and experiments.

Figure 5 (b) shows the profile factor K_p. Here, the dashed lines are the maximum and minimum admissible values of K_p for a fully-developed flow profile. All experimental profile factors are below the threshold $K_{p,min} = 0.8$ for small distances which confirms that the swirl disturbance generator provides notable disturbances of axial velocity profiles in addition to the secondary flow. Further, these disturbances persist for long downstream distances. The profile factor for $Re = 6.0 \cdot 10^4$ appears to increase slower in comparison to the experiments with $Re = 4.0 \cdot 10^4$ and the experiments of Eichler and Lederer 2015. In contrast, all turbulence models except the k-ω SST model and the realizable k-ε model provide profile factors within the admissible range, even at $12.0D$ downstream. This substantiates the view that the tested turbulence models with exception of the realizable k-ε model are not able to provide accurate predictions of axial profiles of swirling flow.

The asymmetry factor is shown in Figure 5 (c). Here, the dashed line represents the maximum admissible value $(K_a = 1\,\%)$ for a fully-developed flow profile according to Eichler and Lederer 2015. We find the highest asymmetry factor for the measurement in the cross-section located at $50.0D$. Only the laminar measurement shows a K_a higher than $1\,\%$, pointing towards the presence of a significant asymmetry in the axial flow profile. All considered turbulence models appear to provide asymmetry factors below $1\,\%$ that do not capture the behavior observed in the experiments. However, the simulations are symmetric by definition, whereas the experiments can develop large-scale asymmetries if the flow becomes unstable.

Panel (d) of Figure 5 shows the turbulence factor K_{Tu}. The experimental results of Eichler and Lederer 2015 (Ref1) indicate a decrease in the region from $12.0D$ to $50.0D$ whereas the present experiments indicate an increase for the same region. Ref1 reaches an acceptable turbulence factor at $50.0D$ but the present experiments not before $105.0D$. Furthermore, Ref1 exhibits a relatively low K_{Tu} at $87.0D$ whereas the present experiments at $Re = 4.0 \cdot 10^4$ show a high K_{Tu} at $105.0D$. Consequently, K_{Tu} appears to comply with the established guidelines, but for a realistic interpretation of results, it is important to realize that the accuracy of K_{Tu} is compromised by the measurement uncertainty of the experiments and a high modeling uncertainty associated with assumptions in the turbulence closures. The numerical results show a high scatter between different models. The realizable k-ε provides increased values, whereas the two k-ω models predict very low K_{Tu} factors. In contrast, the k-ε model and the RNG k-ε model perform better for the prediction of K_{Tu}.

Conclusions and outlook

A comparison between experiments and simulations of disturbed pipe-flow using a standardized swirl disturbance generator was realized. We presented simulation results of the realizable k-ε model, for which we found good agreement of velocity profiles with the experimental data. However, this model only provides reasonable predictions for two performance indicators (K_p and the swirl angle ϕ), while it shows a departure from the experimental results for the asymmetry factor K_a and the turbulence factor K_{Tu}. The discrepancies in K_a can be explained through large-scale asymmetries resulting from instabilities that are not captured with steady-state RANS models. Similarly, the discrepancies in K_{Tu} can be explained with uncertainties in the model formulations, since K_{Tu} is computed from the turbulent kinetic energy that is based on closure approximations in the transport equations. In general, we find that CFD simulations provide a useful practical tool to estimate velocity profiles and associated performance indicators but experimental validation is needed to select suitable models. In other words, a "blind prediction" without knowledge of experimental data is presently not feasible with RANS models for this type of flow. Further, computational time is still a bottleneck for industry applications, in particular if accurate results at distant downstream locations are required. The present CFD simulations were limited to a computational domain covering a distance of $13.0D$ downstream from the swirl disturbance generator. However, considering longer computational domains appears to be well worth the effort and should be realized in future investigations.

Acknowledgement

The authors gratefully acknowledge technical support from Salim Umar and Karsten Lundsgaard.

References

del Olmo Díaz, D., Hinz, D.F., 2015: "Performance of eddy-viscosity turbulence models for predicting swirling pipe-flow: Simulations and laser-Doppler velocimetry". In preparation

Eichler, T., Lederer, T., 2015: "Flow development behind a swirl generator in a hot-water standard measuring facility for large volume rates", Flow Measurement and Instrumentation, 42, pp. 90-97

EN 14154-3:2005+A2:2011, 2011: "Water meters – Part 3: Test methods and equipment", third ed.

Gersten, K., Herwig, H., 1992: "Strömungsmechanik: Grundlagen der Impuls-, Wärme- und Stoffübertragung aus asymptotischer Sicht", Springer Verlag, first ed.

OIML R 49-2:2013, 2013: "International Recommendation: Water meters for cold potable water and hot water, Part 2: Test methods"

Gersten, K., Papenfuss, H.-D., 2005: "Decay of disturbances in turbulent pipe flow", in Fluid Mechanics of Flow Metering, Springer Verlag, ed. Merzkirch, W., pp. 23-47

Müller, U., Dues, M., 2007: "Vollflächige Erfassung von ungestörten und gestörten Geschwindigkeitsverteilungen in Rohrleitungen mittels der Laser-Doppler-Velocimetrie", Technisches Messen, 74, pp. 342-352

Yeh, T.T., Mattingly, G.E., 1994: "Pipe flow downstream of a reducer and its effects on flowmeters", Flow Measurement Instrumentation, 5, p. 181-7

Zagarola, M.V., Smits A.J., 1998: "Mean-flow scaling of turbulent pipe flow", Journal of Fluid Mechanics, 373, pp. 33-79